The Astrophysical Journal Letters, 969:L14 (12pp), 2024 July 1 https://doi.org/10.3847/2041-8213/ad55cd

Discovery of the Optical and Radio Counterpart to the Fast X-Ray Transient EP 240315a

J. H. Gillanders[1,13], L. Rhodes[1,13], S. Srivastav[1,13], F. Carotenuto[1], J. Bright[1], M. E. Huber[2], H. F. Stevance[1,3], S. J. Smartt[1,3], K. C. Chambers[2], T.-W. Chen[4], R. Fender[1,5], A. Andersson[1], A. J. Cooper[1], P. G. Jonker[6], F. J. Cowie[1], T. de Boer[2], N. Erasmus[7], M. D. Fulton[3], H. Gao[2], J. Herman[2], C.-C. Lin[2], T. Lowe[2], E. A. Magnier[2], H.-Y. Miao[4], P. Minguez[2], T. Moore[3], C.-C. Ngeow[4], M. Nicholl[3], Y.-C. Pan[4], G. Pignata[8], A. Rest[9,10], X. Sheng[3], I. A. Smith[11], K. W. Smith[3], J. L. Tonry[2], R. J. Wainscoat[2], J. Weston[3], S. Yang[12], and D. R. Young[3]
[1] Astrophysics sub-Department, Department of Physics, University of Oxford, Keble Road, Oxford, OX1 3RH, UK; james.gillanders@physics.ox.ac.uk, lauren.rhodes@physics.ox.ac.uk, shubham.srivastav@physics.ox.ac.uk
[2] Institute for Astronomy, University of Hawai'i, 2680 Woodlawn Drive, Honolulu, HI 96822, USA
[3] Astrophysics Research Centre, School of Mathematics and Physics, Queen's University Belfast, BT7 1NN, UK
[4] Graduate Institute of Astronomy, National Central University, 300 Jhongda Road, 32001 Jhongli, Taiwan
[5] Department of Astronomy, University of Cape Town, Private Bag X3, Rondebosch 7701, South Africa
[6] Department of Astrophysics/IMAPP, Radboud University, P.O. Box 9010, 6500 GL, Nijmegen, The Netherlands
[7] South African Astronomical Observatory, PO Box 9, Observatory 7935, Cape Town, South Africa
[8] Instituto de Alta Investigación, Universidad de Tarapacá, Arica, Casilla 7D, Chile
[9] Space Telescope Science Institute, 3700 San Martin Drive, Baltimore, MD 21218, USA
[10] Department of Physics and Astronomy, Johns Hopkins University, Baltimore, MD 21218, USA
[11] Institute for Astronomy, University of Hawai'i, 34 Ohia Ku St., Pukalani, HI 96768-8288, USA
[12] Henan Academy of Sciences, Zhengzhou 450046, Henan, People's Republic of China
Received 2024 April 16; revised 2024 June 5; accepted 2024 June 6; published 2024 June 26

Abstract

Fast X-ray Transients (FXTs) are extragalactic bursts of soft X-rays first identified $\gtrsim$10 yr ago. Since then, nearly 40 events have been discovered, although almost all of these have been recovered from archival Chandra and XMM-Newton data. To date, optical sky surveys and follow-up searches have not revealed any multiwavelength counterparts. The Einstein Probe, launched in 2024 January, has started surveying the sky in the soft X-ray regime (0.5–4 keV) and will rapidly increase the sample of FXTs discovered in real time. Here we report the first discovery of both an optical and radio counterpart to a distant FXT, the fourth source publicly released by the Einstein Probe. We discovered a fast-fading optical transient within the 3′ localization radius of EP 240315a with the all-sky optical survey ATLAS, and our follow-up Gemini spectrum provides a redshift, $z = 4.859 \pm 0.002$. Furthermore, we uncovered a radio counterpart in the S band (3.0 GHz) with the MeerKAT radio interferometer. The optical (rest-frame UV) and radio luminosities indicate that the FXT most likely originates from either a long gamma-ray burst or a relativistic tidal disruption event. This may be a fortuitous early mission detection by the Einstein Probe or may signpost a mode of discovery for high-redshift, high-energy transients through soft X-ray surveys, combined with locating multiwavelength counterparts.

Unified Astronomy Thesaurus concepts: Transient sources (1851); Relativistic jets (1390); High energy astrophysics (739); X-ray transient sources (1852); Optical identification (1167); Radio interferometry (1346)

1. Introduction

In the past decade, a few tens of fast X-ray transients (FXTs) have been discovered with Chandra, XMM-Newton, and eROSITA (see, e.g., Jonker et al. 2013; Glennie et al. 2015; Bauer et al. 2017; Alp & Larsson 2020; Quirola-Vásquez et al. 2022, 2023). These bursts are soft (0.3–10 keV) and exhibit a wide range of timescales, lasting from $\sim 10^1$ to 10^4 s, with a variety of astrophysical interpretations having been invoked to explain their properties.

Events such as CDF-S XT2 (Xue et al. 2019), XRT 210423 (Ai & Zhang 2021; Eappachen et al. 2023), and CDF-S XT1 (Sarin et al. 2021) have been interpreted as resulting from a binary neutron star (BNS) merger. CDF-S XT2 and XRT 210423 both showed a clear plateau in the X-ray light curve, followed by a sharp drop, consistent with model predictions for a rapidly spinning magnetar remnant. On the other hand, XRT 000519 showed precursor X-ray emission 4000 and 8000 s before the main flare (Jonker et al. 2013), the timescale of which agrees with the expected orbital timescale of a white dwarf (WD) spiraling toward an intermediate-mass black hole on an eccentric orbit (MacLeod et al. 2016). Glennie et al. (2015) found two FXTs in archival Chandra data and reported an infrared (IR) Galactic counterpart at a distance of 80 pc for one of them (XRT 120830). They interpret this FXT to be consistent with an M dwarf superflare, but the other had no detected counterpart.

Alp & Larsson (2020) reported 12 FXTs from XMM-Newton, and from inference of potential hosts they interpret the FXTs as emission from shock breakout (SBO) in Wolf–Rayet stars within a dense circumstellar medium or (favored in two cases) red supergiant progenitors. Eappachen et al. (2024) showed that seven of these have plausible host galaxies with spectroscopic redshifts $0.098 < z < 0.645$, with one being a likely Galactic flare star. They proposed that one FXT (XRT 110621) is consistent with being a supernova SBO, but the spectroscopic redshifts of the others showed that their peak

[13] These authors contributed equally to this work.

X-ray luminosities were above that deemed feasible for supernova SBOs. Soderberg et al. (2008) report an X-ray detection that they associate with the SBO from SN 2008D, at a distance of 27 Mpc (see also Chevalier & Fransson 2008; Mazzali et al. 2008; Modjaz et al. 2009). Eappachen et al. (2024) also searched for contemporaneous optical counterparts in the Pan-STARRS and Asteroid Terrestrial-impact Last Alert System (ATLAS) wide-field surveys but found none. The detection limits range in depth (from $m_w \simeq 22$ to $m_o \simeq 18.4$; AB mag), and the delay between the bursts and the observations ranges from 1 to 170 days. The most stringent limit on any contemporaneous optical emission remains the serendipitous observation of the location of CDF-S XT 1 with the Very Large Telescope just 80 minutes after the burst (Bauer et al. 2017). With this observation, no associated optical counterpart—or host galaxy—was detected, down to a limiting R-band magnitude $m_R > 25.7$ AB mag.

The discovery and rapid follow-up of FXTs are expected to accelerate since the launch of the Einstein Probe (EP; Yuan et al. 2022) on 2024 January 9. With its instantaneous wide field of view of 3600 deg^2, the mission is designed to survey the available night-time sky several times per day in the soft X-ray regime (0.5–4 keV) and to follow up detected transients. During its commissioning phase, it has already proven to be a valuable discovery instrument, with four new X-ray transient sources reported by mid-March. The first, EPW 20240219aa (Zhang et al. 2024b), has had no multi-wavelength counterpart identified, but an association with a subthreshold Fermi Gamma-ray Burst Monitor (GBM) detection has been made (Zhang et al. 2024a; Fletcher et al. 2024), suggesting that it may be a GRB event. The following two EP transients released are almost certainly Galactic. EPW 20240305aa (Liu et al. 2024b) has been well localized by Swift/XRT (Liu et al. 2024a) and is coincident with a Gaia DR3 star (late A type or early F type; Monageng et al. 2024), with radio emission observed by the Australian Telescope Compact Array (ATCA; An et al. 2024). EP 240309a was detected as a highly variable X-ray source (previously detected by XMM-Newton, Swift, and eROSITA; Ling et al. 2024) and has been confirmed as a cataclysmic variable (CV) with an orbital period of 3.76 hr (Buckley et al. 2024; Rodriguez & Kulkarni 2024).

The fourth bright transient source publicly released by the EP mission, EP 240315a, was detected on 2024 March 15 20:10:44 UTC ($T_0 =$ MJD 60384.84079) by the wide-field X-ray telescope (Zhang et al. 2024c). The EP team reported that the event lasted 1600 s, with a peak flux $f_X \sim 3 \times 10^{-9}$ erg s^{-1} cm^{-2} in the 0.5–4 keV band. No previously known X-ray sources were identified in the 3′ localization radius, making it a candidate extragalactic FXT.

In this Letter, we report the discovery of the optical and radio transient associated with EP 240315a, the first time multi-wavelength counterparts of a "distant" ($D \gtrsim 100$ Mpc) extragalactic FXT have been recorded. Throughout this Letter we assume ΛCDM cosmology with a Hubble constant $H_0 = 67.7$ km s^{-1} Mpc^{-1}, $\Omega_M = 0.309$, and $\Omega_\Lambda = 0.691$ (Planck Collaboration et al. 2016). We also assume a line-of-sight Milky Way extinction of $E(B-V) = 0.042$ AB mag, which corresponds to $A_V = 0.130$ AB mag (Schlafly & Finkbeiner 2011).

2. Multiwavelength Counterpart Discovery and Follow-Up

2.1. Discovery of the Optical Counterpart with ATLAS

ATLAS (Tonry et al. 2018b) is a quadruple 0.5 m telescope system, operating a wide-field all-sky survey. ATLAS continually surveys the sky, typically four times in 24 hr when all four units are operating normally, and we promptly process the data to search for extragalactic transients (Smith et al. 2020). During its normal survey operations, ATLAS observed the localization region of EP 240315a at MJD 60384.894,[14] corresponding to $T_0 + 1.28$ hr (note that the first of the four 30 s exposures was obtained at MJD 60384.88673, or $T_0 + 1.10$ hr). Recall that T_0 is the time of the detection from the EP (MJD 60384.84079; Zhang et al. 2024c).

Observations were performed by the Sutherland unit in South Africa, with 4×30 s exposures obtained using the *cyan*, or *c*, filter (analogous to the Pan-STARRS/Sloan Digital Sky Survey $g + r$ filters). During automated image processing (outlined by Smith et al. 2020), the observations were reduced and calibrated photometrically and astrometrically with the reference catalog RefCat2 (Tonry et al. 2018a), and a reference image was subtracted. We registered the optical transient AT 2024eju (ATLAS24dsx) with sky coordinates of R.A. $= +141.64763$, decl. $= -9.53401$ ($9^h26^m35\overset{s}{.}43$, $-9°32'02\overset{''}{.}4$) and an observed magnitude $m_c = 19.38 \pm 0.08$ AB mag on the Transient Name Server (Tonry et al. 2024). With no detection of the source in ATLAS images 1.75 days before, no historical variability, and a $0\overset{''}{.}8$ spatial separation, we reported this as a plausible counterpart to EP 240315a (Srivastav et al. 2024b).

In Figure 1, we present the nightly stacked (4×30 s) target and difference images from ATLAS for the detection epoch and the neighboring epochs immediately pre- and post-detection. The presence of the transient on MJD 60384.894 is unmistakable, with no evidence for AT 2024eju in the most recent previous observation (indicating no preexisting transient activity) and no evidence in the subsequent observation (indicating its rapid fade). Figure 1 visually highlights how rapidly AT 2024eju rose and subsequently faded.

2.2. Optical Photometric Follow-Up

After the initial discovery with ATLAS, we triggered rapid multiband follow-up imaging observations with the Pan-STARRS telescopes, the Liverpool Telescope, and the Lulin Observatory. All three observatories were triggered and on-source within 24–36 hr.

We used the 40 cm SLT located at Lulin Observatory, Taiwan, to obtain r-band images of the field of EP 240315a as part of the Kinder project (Chen et al. 2021). The initial observation with SLT began at MJD 60385.673, or $T_0 + 0.832$ days. We successfully recovered AT 2024eju in the images, albeit with a marginal detection (Chen et al. 2024a), indicating a fast fade within the first 24 hr of the FXT discovery. Subsequently, we conducted continuous observations of AT 2024eju using both SLT and the Lulin One-meter Telescope (LOT) with i-band imaging. We employed the Kinder pipeline (Yang et al. 2021) to conduct point-spread function (PSF) photometry for AT 2024eju without template subtraction. The derived magnitudes and 2σ upper limits were

[14] Here (and for all other optical imaging observations) we quote the epoch of observation as the midpoint of the exposure.

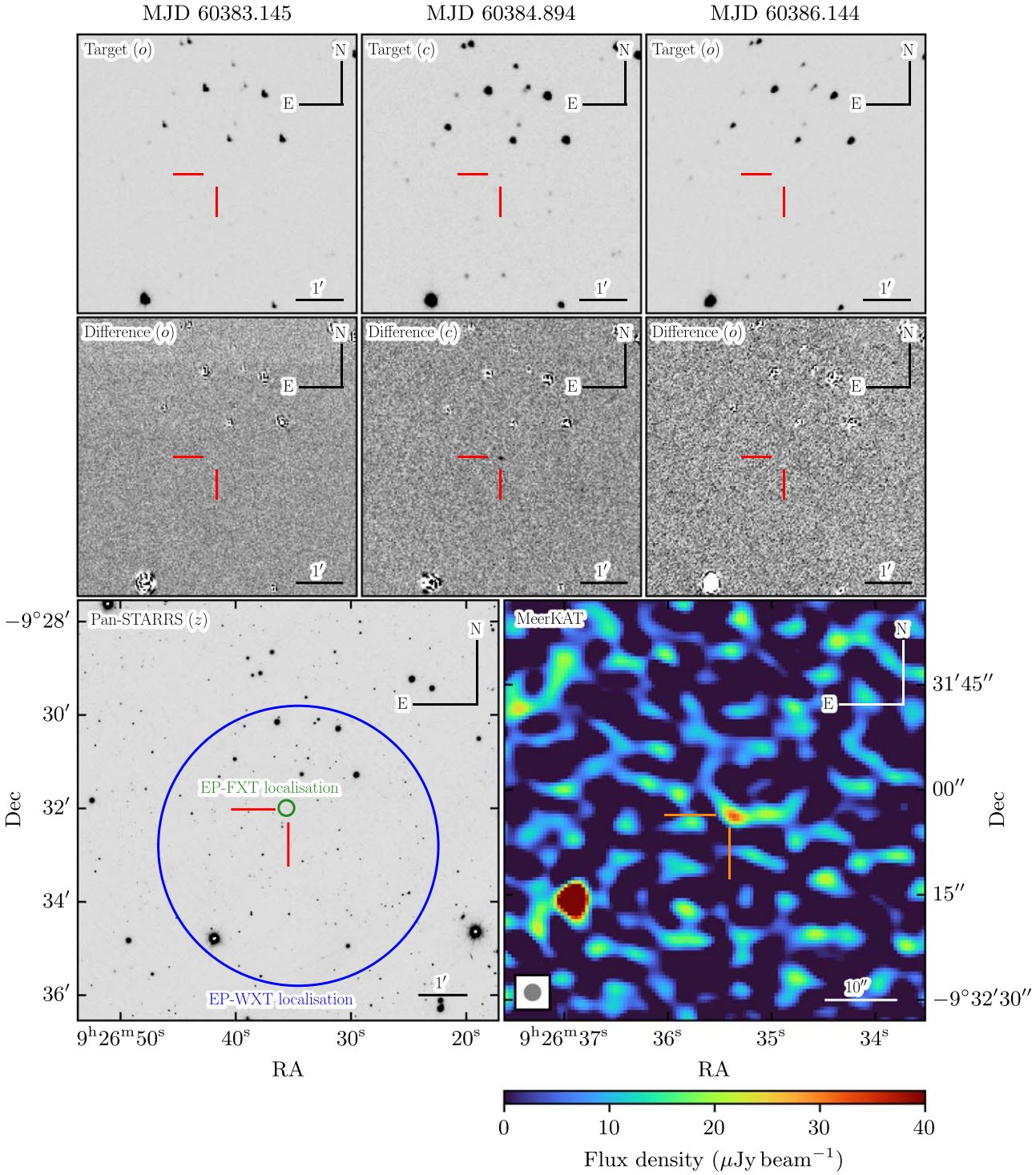

Figure 1. The location of the counterparts to EP 240315a, marked with cross-hairs (red for the optical location from ATLAS, orange for the radio location from MeerKAT). Top panels: ATLAS stacked (4 × 30 s) target images of the field of AT 2024eju. Left to right: *o*-band observation taken at $T_0 - 1.696$ days, detection *c*-band observation taken at $T_0 + 0.054$ days, and the subsequent *o*-band observation taken at $T_0 + 1.304$ days. AT 2024eju faded below the detection threshold of ATLAS in $\lesssim$1.2 days ($m_o > 21.1$ AB mag; 2σ upper limit). Middle panels: same as the top panels, but here we present the difference images. In the center panel, the presence of AT 2024eju is unmistakable. Bottom left panel: Pan-STARRS *z*-band image of the field of AT 2024eju, with the localization regions from the detections of EP 240315a by the EP-WXT (blue; from Zhang et al. 2024c) and EP-FXT (green; from Chen et al. 2024b) overlaid, to illustrate the spatial coincidence with the optical counterpart AT 2024eju. Bottom right panel: MeerKAT radio image of the field of EP 240315a. There is clear evidence for a bright radio source in the image, coincident with EP 240315a. The beam size for the observations is $3\farcs5 \times 3\farcs5$, illustrated by the stamp in the lower left corner. Note the much smaller scale in this image compared with the optical images.

determined by calibrating against Pan-STARRS1 field stars in the AB system.

The 2 m Liverpool Telescope (LT; Steele et al. 2004) was triggered under the program PL24A28 (PI: S. Srivastav). Images were obtained in *gri* bands commencing on MJD 60385.848, corresponding to $T_0 + 1.007$ days. While the observing conditions were poor and the optical counterpart was not detected, our upper limit from non-detections

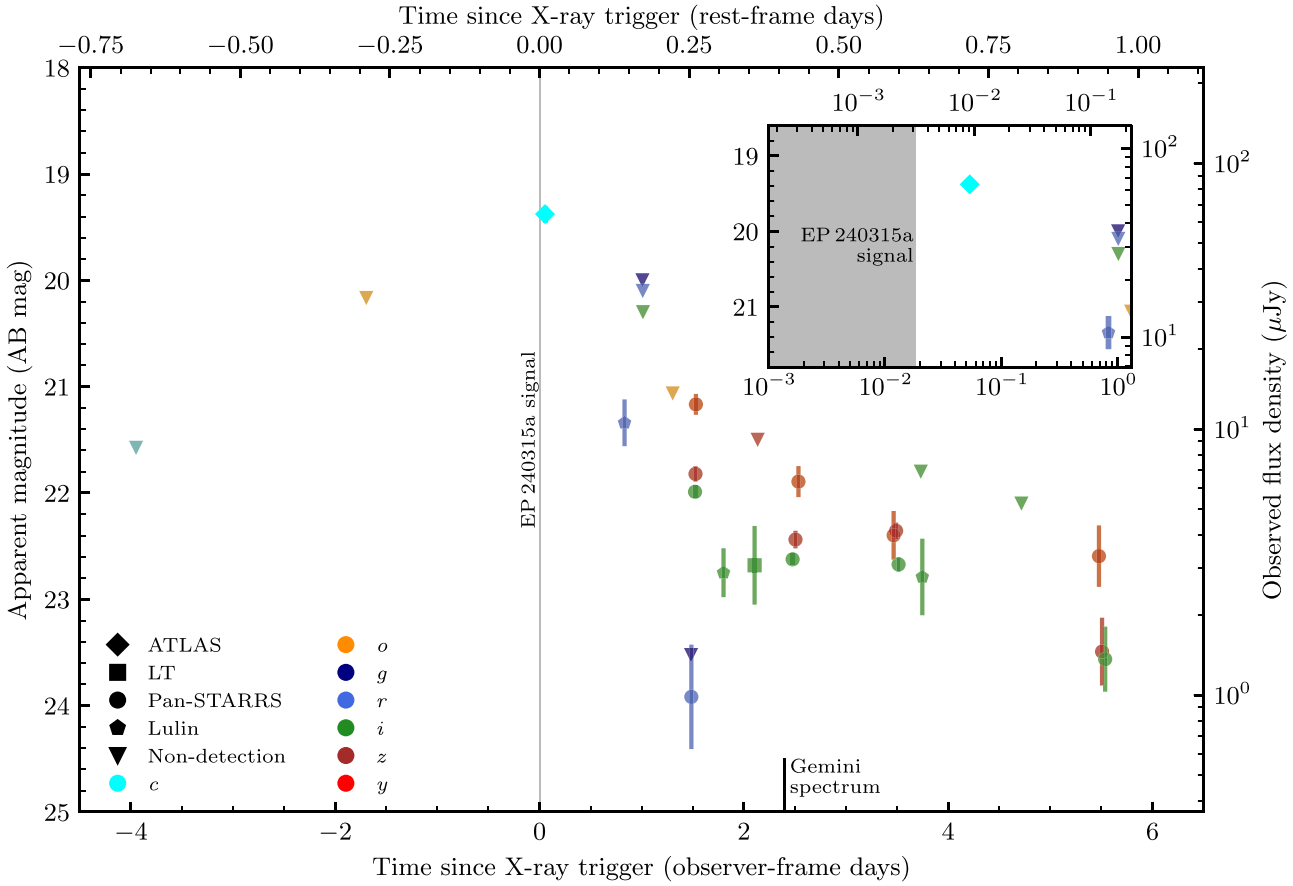

Figure 2. Optical photometry of AT 2024eju. All non-detections are represented by downward-pointing triangles (and correspond to 2σ upper limits). Error bars correspond to 1σ values. We present the data in both observer and rest frame and the flux in both magnitude and f_ν space. The gray band represents the duration of the initial X-ray detection reported by the EP (≈1600 s; see Zhang et al. 2024c). The epoch of spectroscopic observation with Gemini North has also been marked (vertical black line). Inset: a zoom-in of the first ∼1.5 days to emphasize how close our ATLAS *c*-band detection was to the initial X-ray detection (≲80 observer-frame minutes, ≲800 rest-frame seconds). Note that we do not plot the late-time (T_0 + 18.42 days, observer frame) Gemini non-detections.

confirmed the rapidly fading nature of AT 2024eju (see Srivastav et al. 2024a). Another set of *iz*-band images were obtained the next night, at MJD 60386.946, in better conditions. However, given the continuing rapid fade, AT 2024eju was only detected in *i* band. The derived magnitudes and 2σ upper limits from the LT images were estimated using the Python-based `Photometry Sans Frustration` code[15] (Nicholl et al. 2023).

Pan-STARRS observations commenced on MJD 60386.324, or $T_0 + 1.483$ days. The Pan-STARRS system is a twin 1.8 m telescope system (Pan-STARRS1 and Pan-STARRS2), both situated atop Haleakala mountain on the Hawaiian island of Maui (Chambers et al. 2016). All observations of AT 2024eju were performed with Pan-STARRS1 (PS1), which has a 1.4 gigapixel camera and 0.″26 pixels. This provides a focal plane with a diameter of 3.°0 and a field-of-view area of 7.06 deg^2, which can be imaged with the *grizy* filter system (as described by Tonry et al. 2012a). Images were processed with the Image Processing Pipeline (IPP; Magnier et al. 2020a; Waters et al. 2020). The individual exposure frames were astrometrically and photometrically calibrated (Magnier et al. 2020b) and overlapping exposures co-added together with median clipping applied (to produce stacks) on which PSF photometry was performed (Magnier et al. 2020c). We commenced targeted observations on MJD 60386.324 ($T_0 + 1.483$ days). Two epochs of observations were obtained on the first night, with the initial *grizy* followed ∼1.4 hr later by *izy* imaging. We dropped the *gr* bands from all subsequent follow-up, due to the non-detections in our first epoch.

Finally, we obtained an epoch of late-time *iz*-band imaging with the Gemini North/GMOS-N instrument, under the program ID GN-2024A-Q-221 (PI: M. Huber), at MJD 60403.257 ($T_0 + 18.42$ days). These observations were reduced using the `DRAGONS` pipeline (Labrie et al. 2023a, 2023b) and following standard recipes. AT 2024eju was not detected in these deep stacked images, and the 2σ upper limits were again derived using the `PSF` code.

The full optical light curve information, including our ATLAS, Lulin, LT, Pan-STARRS, and Gemini photometry, is presented in Figure 2 and Table 1.

2.3. Spectroscopic Observation with Gemini and Redshift Measurement

In addition to the rapidly acquired photometric data, we obtained a spectrum of the optical counterpart to EP 240315a, commencing on MJD 60387.236 ($T_0 + 2.395$ days). Our observation was carried out using the Gemini North/GMOS-N instrument under program ID GN-2024A-Q-128 (PI: M. Huber) using the R400 grating and 1″ slit width, which provided coverage over the ≈4200–9100 Å wavelength range. Our

[15] https://github.com/mnicholl/photometry-sans-frustration

Table 1
Optical and Radio Photometry of AT 2024eju

Optical					
$T_{mid} - T_0$ (days)	MJD	Telescope	Total Exposure Time (s)	Filter	Apparent Magnitude (AB mag)
−3.950	60380.891	ATLAS	120	*c*	>21.6
−1.696	60383.145	ATLAS	120	*o*	>20.2
+0.054	60384.894	ATLAS	120	*c*	19.38 ± 0.08
+0.832	60385.673	SLT	1800	*r*	21.34 ± 0.22
+1.007	60385.848	LT	180	*g*	>20.0
+1.010	60385.851	LT	180	*r*	>20.1
+1.012	60385.853	LT	180	*i*	>20.3
+1.304	60386.144	ATLAS	120	*o*	>21.1
+1.483	60386.324	PS	300	*g*	>23.5
+1.486	60386.327	PS	300	*r*	23.92 ± 0.49
+1.522	60386.363	PS	700	*i*	21.99 ± 0.06
+1.527	60386.368	PS	700	*z*	21.82 ± 0.07
+1.531	60386.372	PS	700	*y*	21.17 ± 0.10
+1.801	60386.642	LOT	3000	*i*	22.75 ± 0.23
+2.105	60386.946	LT	2400	*i*	22.68 ± 0.37
+2.135	60386.976	LT	2400	*z*	>22.0
+2.477	60387.318	PS	2000	*i*	22.62 ± 0.06
+2.505	60387.346	PS	2000	*z*	22.44 ± 0.08
+2.535	60387.375	PS	1600	*y*	21.89 ± 0.15
+3.466	60388.307	PS	1600	*y*	22.40 ± 0.23
+3.491	60388.331	PS	2000	*z*	22.36 ± 0.08
+3.515	60388.356	PS	2000	*i*	22.67 ± 0.07
+3.732	60388.573	SLT	8700	*i*	>21.8
+3.747	60388.588	LOT	9000	*i*	22.79 ± 0.36
+4.717	60389.558	LOT	6000	*i*	>22.1
+5.477	60390.317	PS	2400	*y*	22.59 ± 0.29
+5.507	60390.347	PS	2400	*z*	23.49 ± 0.32
+5.537	60390.378	PS	2400	*i*	23.56 ± 0.31
+18.42	60403.257	Gemini	910	*i*	>25.8
+18.44	60403.276	Gemini	1170	*z*	>25.8

Radio					
$T_{mid} - T_0$ (days)	MJD	Telescope	Central Frequency (GHz)	Flux Density (μJy beam^{-1})	Concatenated Flux Density (μJy beam^{-1})
+2.86	60387.703	MeerKAT	3.06	34 ± 5	···
+5.57	60390.407	e-MERLIN	5.01	<195	70 ± 8
+12.54	60397.375	e-MERLIN	5.01	<240	···

Note. Magnitudes have not corrected for the expected foreground extinction of $E(B-V) = 0.042$ (Schlafly & Finkbeiner 2011). The errors for the optical photometry are quoted to 1σ, while upper limits are quoted to 2σ significance. The radio upper limits are quoted to 3σ. The final radio column contains the result of concatenating the two e-MERLIN non-detections, resulting in a radio detection.

observation was split into a number of subexposures, with a total on-target exposure time of 8880 s.

We reduced our Gemini observation using the DRAGONS pipeline (Labrie et al. 2023a, 2023b) and following standard recipes, with the reduced spectrum calibrated against a standard star. There are a number of narrow absorption lines evident in the spectrum that can be used to estimate the redshift to the system. The reduced spectrum is shown in the top panel of Figure 3. We fit four of these lines as Gaussian absorption components and estimate the centroids of the features. We find that the four absorption features are centered at ≈7259, 7270, 8167, and 8222 Å, which we propose are produced by the N V $\lambda\lambda$1238.821, 1242.804 and Si IV $\lambda\lambda$1393.755, 1402.770 transitions, respectively. With these line identifications, we estimate the redshift of AT 2024eju to be $z = 4.859 \pm 0.002$. There is evidence for prominent Lyα absorption at ≈7125 Å, in good agreement with our redshift estimate (see bottom left panel of Figure 3). In the bottom right panel of Figure 3, we show a composite spectrum of the four absorption features from which we have estimated our redshift. Our derived redshift value is in line with measurements from two GCNs released after the discovery of AT 2024eju ($z \approx 4.859$; see Quirola-Vásquez et al. 2024; Saccardi et al. 2024).

2.4. Radio Observations

We observed the position of EP 240315a with the MeerKAT radio telescope. The observation was performed as part of program SCI-20230907-JB-01 (PI: J. Bright). MeerKAT is a radio interferometer located in the Karoo desert in South Africa and a precursor of the Square Kilometre Array (SKA). The instrument consists of 64 × 13.5 m antennas that are currently equipped with UHF, L-band, and S-band receivers, covering

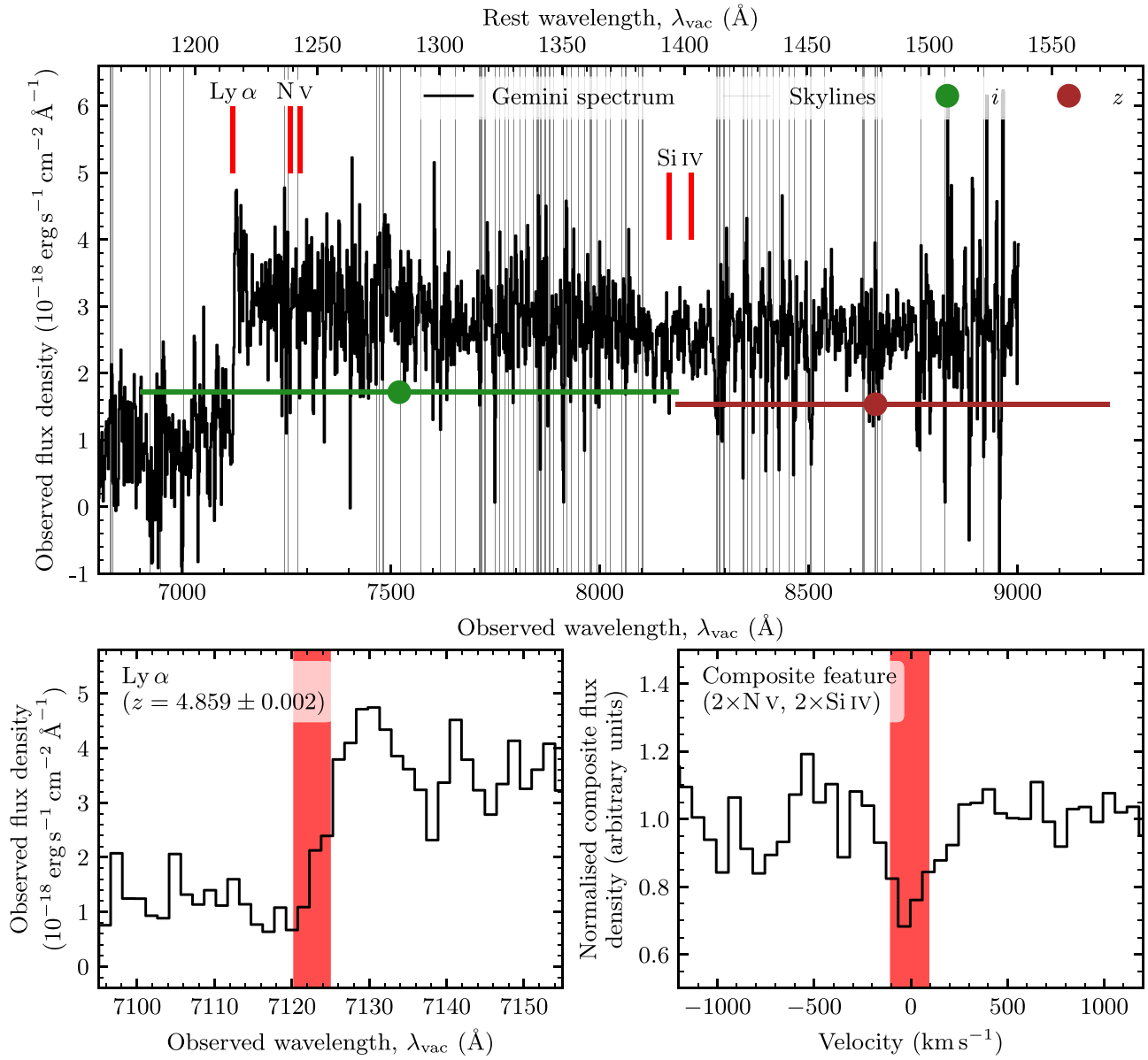

Figure 3. Top panel: Gemini North/GMOS-N telluric-corrected spectrum of EP 240315a/AT 2024eju. The Pan-STARRS *iz*-band observations taken ≈0.1 days after the spectral observations are overlaid. The absorption lines from which we estimate the redshift of the system have been marked (vertical red lines). Prominent skylines (from Hanuschik 2003) have been marked with vertical gray lines. Bottom left panel: a zoom-in on the region of strong Lyα absorption (the width of the red band is representative of our redshift uncertainty). Bottom right panel: composite spectrum of AT 2024eju, constructed from the profiles of the four absorption features we used to measure the redshift to EP 240315a (N v λλ1238.821, 1242.804 and Si iv λλ1393.755, 1402.770). Note that this composite spectrum has been normalized and transformed to velocity space. The width of the red band is again representative of our estimated redshift uncertainty.

the 0.5−3.5 GHz frequency range. Characterized by a dense core and with a longest baseline of 8 km, the array offers an excellent snapshot *uv*-coverage, a large field of view (1.69 deg^2), and roughly microjansky sensitivity (Camilo et al. 2018; Jonas 2018). We observed EP 240315a with MeerKAT starting on MJD 60387.703 ($T_0 + 2.86$ days), for a total on-source time of 42 minutes. We observed at a central frequency of 3.06 GHz (S band, S3), with a total bandwidth of 875 MHz. PKS J1939–6342 and 3C 237 were used as flux and complex gain calibrators, respectively. The data were reduced with the `OxKAT` pipeline (Heywood 2020), which performs standard flagging, calibration, and imaging using `tricolour` (Hugo et al. 2022), `CASA` (CASA Team et al. 2022), and `WSCLEAN` (Offringa et al. 2014), respectively. Specifically, for the imaging part we adopted a Briggs weighting scheme with a −0.3 robust parameter, yielding a $3\farcs5 \times 3\farcs5$ beam and 8 μJy beam^{-1} rms noise in the target field. We clearly detected a point source at the position of the optical counterpart AT 2024eju (first announced by Carotenuto et al. 2024; see also Figure 1). Fitting for a point source in the image plane, we measure a flux density of 34 ± 5 μJy beam^{-1}.

Upon the discovery of a radio counterpart with the MeerKAT radio telescope, we obtained a rapid response time request with the *enhanced*-Multi-Element Radio Linked Interferometer Network (e-MERLIN, DD17004; PI: L. Rhodes). e-MERLIN is a UK-based radio interferometer with a maximum baseline of 217 km and seven dishes spanning 25−76 m in diameter. The facility can observe at L, C, and K band. Given the improved phase stability and sensitivity, we requested that our observation be made at C band with a central frequency of 5.08 GHz and a

Table 2
Wavelength Coverage for the Different Filters/Bands of Our Observations (Both Optical and Radio)

Optical		
Filter	Wavelength (Å, Observer Frame)	Wavelength (Å, Rest Frame)
c	5330^{+1180}_{-1100}	910^{+200}_{-190}
o	6780^{+1410}_{-1170}	1160^{+240}_{-200}
g	4810^{+700}_{-670}	820^{+120}_{-110}
r	6170^{+720}_{-670}	1050^{+120}_{-110}
i	7520^{+670}_{-620}	1280^{+110}_{-100}
z	8660^{+560}_{-480}	1480^{+100}_{-80}
y	9620^{+390}_{-440}	1640^{+70}_{-80}

Radio				
Filter	Central Frequency (GHz, Observer Frame)	Bandwidth	Central Frequency (GHz, Rest Frame)	Bandwidth
S3	3.06	0.88	17.93	5.16
C	5.01	0.51	29.35	2.99

Note. We present the wavelengths/frequencies in both the observer and rest frames, to emphasize the short wavelengths/high frequencies being sampled in the rest frame of the transient. The ATLAS *co*-band wavelength information is taken from Tonry et al. (2018b), while the Pan-STARRS *grizy*-band wavelength information is extracted from Tonry et al. (2012b).

bandwidth of 0.51 GHz. We obtained two observations; the first commenced on MJD 60389.736 ($T_0 + 4.90$ days) and finished on MJD 60391.083 ($T_0 + 6.24$ days), while the second started on MJD 60396.708 ($T_0 + 11.87$ days) and finished on MJD 60398.042 ($T_0 + 13.20$ days), each with a break in the middle while the target was below the horizon. The observations consisted of a series of 6-minute scans of the target field, followed by 2 minutes on the phase calibrator (0933–0819). The target-phase cal loops were bookended by visits to the flux and bandpass calibrators (J1331+3030 and J1407+2827, respectively). The data were flagged, calibrated, and imaged using the e-MERLIN pipeline[16] (Moldon 2021). Using a uniform image weighting, we do not find any radio emission at either epoch, with 3σ upper limits of 195 and 240 μJy beam^{-1}, respectively. However, combining the observations reduced the rms noise to 17 μJy beam^{-1},[17] enabling us to extract a significant detection of 70 ± 8 μJy beam^{-1}.

3. Results and Discussion

The discovery of the optical counterpart AT 2024eju, with its rapidly fading nature and remarkably high redshift ($z = 4.859 \pm 0.002$), represents the first time an extragalactic FXT has been observed at other wavelengths. The redshift means that our optical observations sampled the emitted ultraviolet flux over the first day of its evolution in the source's rest frame. In Table 2, we present the effective wavelength centroids and widths for the filters with which we performed our observations. In the rest frame of the transient, our initial *g*-band observation with Pan-STARRS sampled $\lambda_{\rm rest} = 820^{+120}_{-110}$ Å, and we recovered $m_g > 23.5$ AB mag. With our subsequent redshift estimate extracted from our Gemini spectrum (see Section 2.3), this non-detection is expected, since we sampled wavelengths blueward of the Lyman limit ($\lambda = 911.3$ Å). Even our reddest filter (*y* band) only probed $\lambda_{\rm rest} = 1640^{+70}_{-80}$ Å, a region still well into the UV. Our dense photometric coverage, with intranight cadence (thanks to our coordinated efforts across multiple observatories, strategically placed at different longitudes) from $T_0 + 0.054$ days to $T_0 + 5.537$ days, corresponds to temporal sampling in the rest frame from $T_0 + 13.3$ minutes to $T_0 + 22.7$ hr. Our late-time Gemini observations ($T_0 + 18.42$ observer-frame days) correspond to a rest-frame phase of $T_0 + 3.14$ days.

The radio counterpart from the MeerKAT radio telescope, an unresolved point source with a flux density of 34 ± 5 μJy, is also the first radio source to be associated with an extragalactic FXT. The combination of what is almost certainly nonthermal radio emission, exceptional ultraviolet luminosity, and rapid evolution indicates that EP 240315a is most likely related to physical mechanisms that produce highly relativistic jets rather than slower thermal transients (e.g., Granot & van der Horst 2014; Anderson et al. 2017; Alexander et al. 2020).

3.1. The Early Optical and Radio Fluxes

The optical discovery epoch (the cyan diamond data point in Figure 2) was obtained ~520 s (rest frame) after the EP-WXT stopped detecting the initial X-ray emission. It then faded by ~2 mag within ≈0.13 rest-frame days ($m_c = 19.38 \pm 0.08$ to $m_r = 21.34 \pm 0.22$; AB mag), corresponding to a temporal index of ≈0.9. The combination of proximity in time of the initial ATLAS detection and the X-ray counterpart followed by such a rapid decay could indicate that the earliest optical emission is from the same emitting region and mechanism as the X-ray burst. Similar behavior has been observed in some long GRBs where large field-of-view optical facilities have obtained simultaneous optical and gamma-ray detections (e.g., Vestrand et al. 2005; Racusin et al. 2008). It is important to distinguish between the *prompt* and *afterglow* emission in the optical data to create the most accurate picture of the early-time emission from this system for future modeling efforts. The

[16] https://github.com/e-merlin/eMERLIN_CASA_pipeline

[17] The significant reduction in the rms noise of the concatenated observation is achieved because of our ability to recover otherwise-flagged data that are flagged out during the reduction of the individual images.

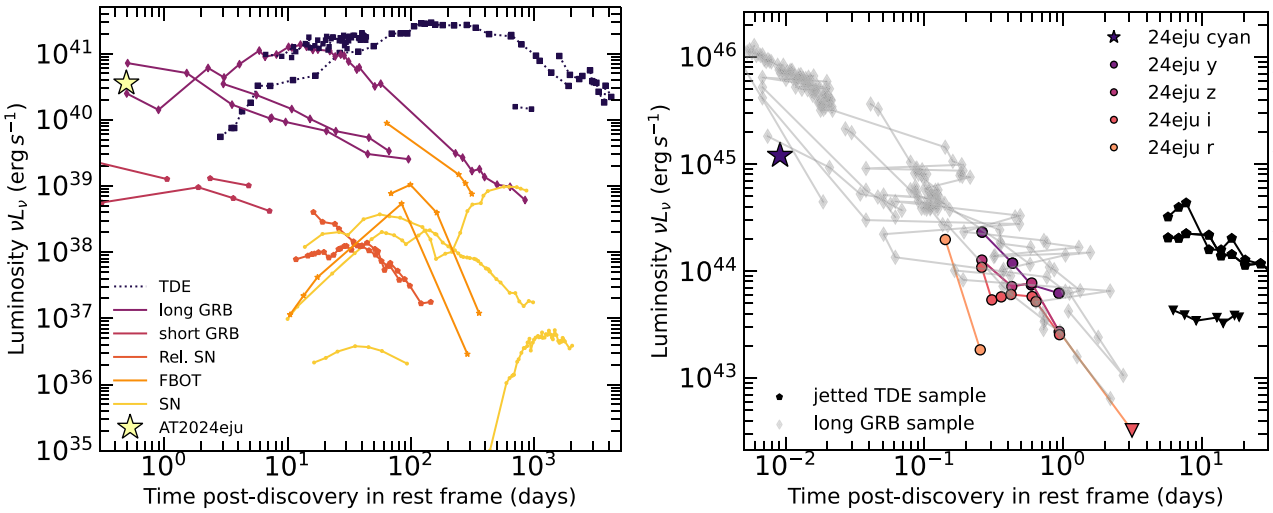

Figure 4. Left panel: radio luminosity of different classes of extragalactic transients adapted from Ho et al. (2020), including data from Laskar et al. (2023) and Rhodes et al. (2023). The yellow star indicates the radio luminosity derived from our MeerKAT detection of EP 240315a. The luminosity is consistent with both GRBs and jetted TDEs. Right panel: AT 2024eju optical (rest-frame UV) detections and Gemini upper limits compared to a sample of rest-frame, UV-detected, long GRB afterglows at redshifts of $z > 2$ (Kann et al. 2010); the UV counterpart of the jetted TDE AT 2022cmc (Yao et al. 2024); and upper limits from the candidate jetted TDE Swift J2058.4 + 0516 (Cenko et al. 2012; Andreoni et al. 2022).

afterglow component of the observed emission appears to flatten, or plateau, in the optical (*izy*) bands.

We combined our e-MERLIN and MeerKAT detections with the published ATCA 5.5 and 9 GHz ∼100 μJy detections (Leung et al. 2024; Ricci et al. 2024) and found that our observations are consistent with self-absorbed synchrotron emission. Given the spectral regime in which our data sits, we expect the radio counterpart to increase in flux density over the coming months.

3.2. What Is the Nature of EP 240315a/AT 2024eju?

Despite our comprehensive follow-up campaign—the first of its kind for an extragalactic FXT—we cannot conclusively determine the origin of EP 240315a. Our observations are consistent with two classes of extragalactic transients: gamma-ray bursts (GRBs) and jetted tidal disruption events (TDEs).

GRBs are identifiable through their highly variable prompt gamma-ray emission, followed by a smoothly evolving synchrotron afterglow, produced as a highly relativistic jet collides with the circumburst environment. GRB 240315C, detected by the Neil Gehrels Swift Observatory/Burst Alert Telescope (Swift/BAT) and Konus Wind (KW) instruments (Svinkin et al. 2024a; DeLaunay et al. 2024), was temporally coincident with EP 240315a. The BAT signal began at $T_0 + 350$ s and was detected at 15–350 keV. The KW signal was detected from $T_0 + 374$ s at 20–1600 keV. The GRB detections lasted ∼70 and 47 s in the BAT and KW data, respectively. The IPN triangulation of GRB 240315C places EP 240315a just within the annulus of 26.°7 width (Svinkin et al. 2024b). Svinkin et al. (2024a) note that the KW detection had an elevated background owing to increased solar flare activity. It is rare, but not completely unprecedented, to have a soft X-ray signal before the GRB itself (see, e.g., Murakami et al. 1991; Piro et al. 2005), although in the case of EP 240315a and GRB 240315C the X-ray duration is significantly longer than in the two previous cases. It is likely that the two signals are related, but further investigation of the high-energy data is required.

It is possible that EP 240315a and GRB 240315C fall within the class of ultralong GRBs. Ultralong GRBs are events whose prompt emission lasts as long as 10,000 s. Like "regular" long GRBs, ultralong GRBs have a large range of afterglow luminosities (see, e.g., Levan et al. 2014, for multiwavelength studies). As such, we cannot rule out the possibility that EP 240315a and GRB 240515C correspond to an ultralong GRB event.

A short GRB (events where the prompt flash of gamma rays is usually *shorter* than ∼2 s)[18] interpretation of EP 240315a requires a BNS merger to have occurred ≈1.2 Gyr after the big bang (derived from $z = 4.859$), assuming standard cosmological parameters, as adopted in Section 1. Canonically dominant evolutionary channels involve an initially tight binary of massive OB stars that undergo two core-collapse supernovae (e.g., Tauris et al. 2017) and crucial common-envelope evolution before coalescence via gravitational inspiral. Binary evolution simulations find a range of peak delay time distributions from $\ll 1$ Gyr in rapid population synthesis (Belczynski et al. 2018; Chruslinska et al. 2018; Vigna-Gómez et al. 2018) to as low as 10 Myr in the BPASS detailed stellar evolution models (Eldridge et al. 2019). Additionally, the cosmic star formation rate (and therefore the merger rate) is suppressed above $z \gtrsim 2$ (Madau & Dickinson 2014; Mapelli & Giacobbo 2018), but many models are consistent with significant BNS merger rates at $z \approx 5$ (Santoliquido et al. 2021). Consequently, we cannot rule out a BNS origin for EP 240315a on the grounds of stellar evolution and inspiral time alone. However, we strongly disfavor the BNS merger/short GRB scenario through the comparison of radio luminosities and timescales. A sample of radio-detected short GRB afterglows is shown in the left panel of Figure 4. Their luminosities are around two orders of magnitude lower than AT 2024eju, making a short GRB an unlikely origin of EP 240315a/AT 2024eju.

Unlike short GRBs, long GRBs (events where the prompt flash of gamma rays is usually *longer* than ∼2 s; see footnote

[18] This inferred duration is detector dependent.

5), produced by collapsing massive stars,[19] occupy a similar region of transient luminosity parameter space. In all wave bands, their afterglow component is more luminous than their short GRB analogs, likely due (at least in part) to higher kinetic energies in the jets of long GRBs compared to short GRBs (Fong et al. 2015; Aksulu et al. 2022). This is demonstrated best in the left panel of Figure 4. The long GRB radio counterparts are approximately two orders of magnitude more luminous than short GRBs. As such, the long GRB radio population is far more consistent with the position of AT 2024eju in the radio luminosity parameter space. A similar conclusion can be reached regarding the position of AT 2024eju in optical luminosity parameter space. The right panel of Figure 4 shows a sample of optically detected, high-redshift ($z > 2$; therefore rest-frame UV) GRB afterglows, alongside our photometric measurements of AT 2024eju. Their luminosities and evolution are extremely consistent.

Furthermore, the X-ray decay (as reported by Levan et al. 2024b, 2024c) follows $f_X \propto t^{-2.1}$, a decay rate that is consistent with a post-jet-break scenario (which occurs when the bulk Lorentz factor of the jet is less than the inverse of the jet opening angle; Sari et al. 1999; Groh et al. 2013; Wang et al. 2018). However, we note that the spectral slope (photon index $= 1.4 \pm 0.5$) reported by Chen et al. (2024b) is on the hard side of afterglow spectra but has large uncertainties (Grupe et al. 2013). The other main possibility for the origin of EP 240315a is a jetted TDE, also known as a relativistic TDE. There have been two well-studied jetted TDEs and at least two additional candidate events discovered thus far (Burrows et al. 2011; Levan et al. 2011; Cenko et al. 2012; Brown et al. 2015; Andreoni et al. 2022; Pasham et al. 2023). While not all jetted TDEs have optical counterparts, they all have luminous and highly variable X-ray counterparts. In the right panel of Figure 4, we present the values and limits of rest-frame optical/UV jetted TDE observations (in luminosity space), alongside the GRB rest-frame UV detections. Furthermore, all jetted TDEs so far have luminous, long-lasting radio counterparts, consistent with highly relativistic jets (e.g., Zauderer et al. 2011; Rhodes et al. 2023).

At a redshift of $z = 4.859$, the isotropic X-ray luminosity of EP 240315a (from the average unabsorbed 0.5−4.0 keV flux of $5.3^{+1.0}_{-0.7} \times 10^{-10}$ erg s^{-1} cm^{-2}, as reported by Zhang et al. 2024c) is $L_X \simeq (1.3 \pm 0.2) \times 10^{50}$ erg s^{-1}, over the rest-frame 3–23 keV band. This sits at the top end of the luminosity range for the X-ray flares associated with Swift J1644. The X-ray decay and the photon index measurements are also similar (Burrows et al. 2011; Levan et al. 2024c). The first optical data point of AT 2022cmc from Andreoni et al. (2022) was acquired 1 day post-burst (rest frame), which is later than the detections of AT 2024eju we report here. However, extrapolation of the AT 2022cmc detections shows that they are consistent with the results we report here for AT 2024eju.

[19] We acknowledge the growing evidence for a population of merger-GRB events, including GRB 211211A (Rastinejad et al. 2022; Troja et al. 2022; Yang et al. 2022; Gompertz et al. 2023) and GRB 230307A (Gillanders et al. 2023; Sun et al. 2023; Levan et al. 2024a; Yang et al. 2024), that lie within the long GRB $T_{90} \gtrsim 2$ s parameter space, where T_{90} is the time between the burst emitting 5% and 95% of the detected counts. However, here we are referring to the *traditional* progenitor system picture, where short GRBs are produced by compact object mergers and long GRB events are produced by massive-star core collapse.

At radio frequencies, both Swift J1644 and AT 2022cmc have reported luminous, slowly evolving counterparts, as shown in the left panel of Figure 4. The radio emission comes from external shocks between the jet and the circumnuclear environment. The radio detection of AT 2024eju, while made earlier than for the other jetted TDEs presented, occupies the same luminosity parameter space.

EP 240315a has characteristics that would allow it to be classified as either a GRB or a jetted TDE. Figure 4 illustrates where our radio and optical discoveries sit compared to other extragalactic transients that have been detected in both the radio and optical bands. Currently, it is not possible to differentiate between the TDE or GRB scenarios. Radio observations of both GRBs and jetted TDEs have found optically thick counterparts at early times (Bright et al. 2023; Rhodes et al. 2023), consistent with our findings here.

In the rest-frame UV, all of our detections are consistent with the low-luminosity end of the GRB afterglow distribution. There are no detections of jetted TDEs at such early times. The earliest UV detection of a jetted TDE recorded is roughly a few days post-burst (rest frame; Yao et al. 2024), later than our final optical detection. Furthermore, only one jetted TDE has been detected in the UV. The other event only has upper limits (Cenko et al. 2012), an order of magnitude below the detections. This range demonstrates the large possible range of UV parameter space associated with TDEs that is still to be explored, making it very hard to estimate the early UV properties of the jetted TDE family.

We rule out the possibility of AT 2024eju being a transient similar to a fast blue optical transient (FBOT) based on the mismatch between the early evolution of this FXT and that of AT 2018cow, the prototypical FBOT transient. While the peak bolometric luminosity of AT 2018cow roughly matches the early follow-up observations of AT 2024eju ($L_{bol} \sim 10^{44}$ erg s^{-1}; Prentice et al. 2018), the rise time is much slower: $t_{rise} \simeq 3$ rest-frame days, versus $\simeq$0.3 rest-frame days for AT 2024eju. Additionally, the early radio light curve of AT 2018cow demonstrates a slow rise to maximum radio luminosity of $\sim$100 rest-frame days (see, e.g., Ho et al. 2019), which does not match the early, very luminous radio detection for EP 240315a. This FXT event evolves on a much more rapid timescale than AT 2018cow, in both the optical and radio, leading us to rule out FBOTs as an explanation for this transient.

3.3. Archival Search for Other Orphan Fast-evolving Optical Transients

Fast-fading transients are commonly found by ATLAS and the Zwicky Transient Facility (ZTF; Bellm et al. 2019), some of which may be extragalactic counterparts to GRBs or FXTs (Stalder et al. 2017; Andreoni et al. 2021). However, the main issue with identifying such transients is the foreground contamination rate of fast CVs, which also often have no host star in Pan-STARRS or Legacy Survey images. In the ATLAS database, there have been $\sim$400 objects flagged as high-significance transients with no cataloged host (Smith et al. 2020).

We manually checked all of these objects and found that most had decay rates that were too slow to match AT 2024eju (likely supernovae or relatively common CVs) or were characteristic of stellar variability with low signal-to-noise ratios. We found 34 genuine orphans detected on only one

night, with signs of rapid fading (evidenced by a non-detection in quick succession to the sole epoch of detection). However, the constraints on their rate of fading still do not allow them to be confidently separated from Galactic CVs. Only by combining with external triggers, such as the EP, will we be able to build a better understanding of the optical counterparts to extragalactic FXTs.

4. Summary and Conclusions

In this Letter we presented the discovery of the optical and radio counterparts to the EP FXT EP 240315a.

The optical counterpart, AT 2024eju, was detected as a hostless transient by ATLAS during its routine all-sky survey operations just 0.054 days (1.28 hr) after the X-ray signal recorded by the EP. We recorded a non-detection 1.7 days prior to discovery and constrained its rapid fade, with it decaying by $\sim$2 mag in 19 hr post-discovery (see Figure 1).

The radio counterpart to EP 240315a was discovered by the MeerKAT radio telescope 2.86 days after the X-ray signal was recorded and has been shown to originate from optically thick synchrotron emission by follow-up complementary e-MERLIN observations.

Our measured redshift ($z = 4.859 \pm 0.002$) rules out some of the models proposed for FXTs, including supernova SBOs, BNS mergers, and tidal disruption of WDs. The inferred high luminosity of the X-ray, optical, and radio emission implies that this is a relativistic event, and we propose two possible scenarios: a long GRB or a jetted TDE.

To differentiate between the GRB and TDE scenarios, continued monitoring of EP 240315a is needed in both the radio and optical bands. The evolutionary timescale of the afterglow is a clear differentiating feature of GRBs from TDEs, as GRBs evolve much more rapidly—usually decaying on a timescale of roughly days to weeks. If we consider the optical temporal behavior of AT 2022cmc to be characteristic of all jetted TDEs, then the TDE light curve should plateau. Our Gemini upper limits, obtained at $T_0 + 18.42$ days post-discovery, are deep enough to rule out an AT 2022cmc-like light curve and luminosity over the same temporal range. The Gemini upper limits favor a GRB-like light curve but are still consistent with the upper limits obtained for Swift J1644 (Bloom et al. 2011).

In the radio band, we predict that differentiating between the TDE and GRB scenarios will take longer, at least 50–100 rest-frame days. The decay rate inferred from the Gemini upper limits seems to prefer the GRB scenario (see Figure 4). However, given the lack of knowledge regarding UV counterparts to jetted TDEs, we cannot confidently rule out the TDE scenario without further observations.

While the majority of long GRBs have been observed to decay in the radio, there are exceptions such as GRB 030329 (Berger et al. 2003; van der Horst et al. 2008), where they continued to rise for weeks post-burst. Fortunately, given the high luminosity of the radio counterpart, even at a redshift of $z = 4.859 \pm 0.002$, it will be possible to track the radio emission for months to years, allowing us to confidently classify this transient with future observations.

While it is difficult to quantify the future rates of such events, the discovery of EP 240315a so soon after the launch of the EP ($\sim$2 months) indicates that such events are probably not intrinsically rare. The soft X-ray regime that EP is optimized to explore is ideal for searching for high-redshift events that emit high-energy radiation, as redshifting will shift the peak of this emission from gamma rays to X-rays, making them more detectable to the EP and other X-ray observatories. The nature of this FXT indicates that the EP will uncover a range of high-energy transient phenomena in both the low- and high-redshift Universe.

Acknowledgments

We thank the anonymous referee for useful comments that helped improve the final version of the manuscript.

We thank Andrew J. Bunker and Alex J. Cameron for useful discussions regarding the interpretation of the redshift of EP 240315a.

We thank L. Piro, G. Bruni, A. Linesh Thakur, and G. Gianfagna for useful discussion surrounding the initial reduction of the e-MERLIN data, which was jointly awarded under two distinct program IDs (DD17003 and DD17004; PIs: G. Bruni, L. Rhodes, respectively).

S.J.S., S.S., K.W.S., and D.R.Y. acknowledge funding from STFC grants ST/Y001605/1, ST/X001253/1, ST/X006506/1, and ST/T000198/1. S.J.S. acknowledges a Royal Society Research Professorship. H.F.S. is supported by the Eric and Wendy Schmidt AI in Science Fellowship. R.F. acknowledges support from STFC, the ERC, and the Hintze Family Charitable Foundation. P.G.J. has received funding from the European Research Council (ERC) under the European Union's Horizon 2020 research and innovation program (grant agreement No. 101095973). M.N. is supported by the European Research Council (ERC) under the European Union's Horizon 2020 research and innovation program (grant agreement No. 948381) and by UK Space Agency grant No. ST/Y000692/1. F.C. acknowledges support from the Royal Society through the Newton International Fellowship program (NIF/R1/211296). A.J.C. acknowledges support from the Hintze Family Charitable Foundation. T.W.C. acknowledges the Yushan Young Fellow Program by the Ministry of Education, Taiwan for the financial support. S.Y. acknowledges the funding from the National Natural Science Foundation of China under grant No. 12303046.

ATLAS is primarily funded through NASA grants NN12AR55G, 80NSSC18K0284, and 80NSSC18K1575. The ATLAS science products are provided by the University of Hawaii, Queen's University Belfast, STScI, SAAO, and Millennium Institute of Astrophysics in Chile.

Pan-STARRS is primarily funded to search for near-Earth asteroids through NASA grants NNX08AR22G and NNX14AM74G. The Pan-STARRS science products for transient follow-up are made possible through the contributions of the University of Hawaii Institute for Astronomy and Queen's University Belfast.

This publication has made use of data collected at Lulin Observatory, partly supported by MoST grant 108-2112-M-008-001. We thank Lulin staff H.-Y. Hsiao, W.-J. Hou, C.-S. Lin, H.-C. Lin, and J.-K. Guo for observations and data management and C.-Y. Cheng for the fringing pattern exam.

The Liverpool Telescope is operated on the island of La Palma by Liverpool John Moores University in the Spanish Observatorio del Roque de los Muchachos of the Instituto de Astrofisica de Canarias with financial support from the UK Science and Technology Facilities Council.

Based on observations obtained at the international Gemini Observatory (under program IDs GN-2024A-Q-221 and GN-

2024A-Q-128), a program of NSF NOIRLab, which is managed by the Association of Universities for Research in Astronomy (AURA) under a cooperative agreement with the US National Science Foundation on behalf of the Gemini Observatory partnership: the US National Science Foundation (United States), National Research Council (Canada), Agencia Nacional de Investigación y Desarrollo (Chile), Ministerio de Ciencia, Tecnología e Innovación (Argentina), Ministério da Ciência, Tecnologia, Inovações e Comunicações (Brazil), and Korea Astronomy and Space Science Institute (Republic of Korea). This work was enabled by observations made from the Gemini North telescope, located within the Maunakea Science Reserve and adjacent to the summit of Maunakea. We are grateful for the privilege of observing the Universe from a place that is unique in both its astronomical quality and its cultural significance.

The MeerKAT telescope is operated by the South African Radio Astronomy Observatory, which is a facility of the National Research Foundation, an agency of the Department of Science and Innovation. This work has made use of the "MPIfR S-band receiver system" designed, constructed, and maintained by funding of the MPI für Radioastronomy and the Max-Planck-Society.

e-MERLIN is a National Facility operated by the University of Manchester at Jodrell Bank Observatory on behalf of STFC.

Facilities: ATLAS, PS1, Gemini:Gillett, Liverpool:2m, MeerKAT, MERLIN, LO:1m

Software: `Astropy` (Astropy Collaboration et al. 2013, 2018, 2022), `Matplotlib` (Hunter 2007), `NumPy` (Harris et al. 2020), `pandas` (McKinney 2010; pandas development team 2020), `DRAGONS` (Labrie et al. 2023a, 2023b), `CASA` (CASA Team et al. 2022), `OxKAT` (Heywood 2020).

ORCID iDs

J. H. Gillanders https://orcid.org/0000-0002-8094-6108
L. Rhodes https://orcid.org/0000-0003-2705-4941
S. Srivastav https://orcid.org/0000-0003-4524-6883
F. Carotenuto https://orcid.org/0000-0002-0426-3276
J. Bright https://orcid.org/0000-0002-7735-5796
M. E. Huber https://orcid.org/0000-0003-1059-9603
H. F. Stevance https://orcid.org/0000-0002-0504-4323
S. J. Smartt https://orcid.org/0000-0002-8229-1731
K. C. Chambers https://orcid.org/0000-0001-6965-7789
T.-W. Chen https://orcid.org/0000-0002-1066-6098
A. Andersson https://orcid.org/0000-0003-2734-1895
A. J. Cooper https://orcid.org/0000-0002-4033-3139
P. G. Jonker https://orcid.org/0000-0001-5679-0695
F. J. Cowie https://orcid.org/0009-0009-0079-2419
N. Erasmus https://orcid.org/0000-0002-9986-3898
M. D. Fulton https://orcid.org/0000-0003-1916-0664
H. Gao https://orcid.org/0000-0003-1015-5367
C.-C. Lin https://orcid.org/0000-0002-7272-5129
E. A. Magnier https://orcid.org/0000-0002-7965-2815
H.-Y. Miao https://orcid.org/0000-0003-2736-5977
T. Moore https://orcid.org/0000-0001-8385-3727
C.-C. Ngeow https://orcid.org/0000-0001-8771-7554
M. Nicholl https://orcid.org/0000-0002-2555-3192
Y.-C. Pan https://orcid.org/0000-0001-8415-6720
G. Pignata https://orcid.org/0000-0003-0006-0188
X. Sheng https://orcid.org/0000-0002-6527-1368
I. A. Smith https://orcid.org/0000-0001-8605-5608
K. W. Smith https://orcid.org/0000-0001-9535-3199
J. L. Tonry https://orcid.org/0000-0003-2858-9657
R. J. Wainscoat https://orcid.org/0000-0002-1341-0952
D. R. Young https://orcid.org/0000-0002-1229-2499

References

Ai, S., & Zhang, B. 2021, ApJL, 915, L11
Aksulu, M. D., Wijers, R. A. M. J., van Eerten, H. J., & van der Horst, A. J. 2022, MNRAS, 511, 2848
Alexander, K. D., van Velzen, S., Horesh, A., & Zauderer, B. A. 2020, SSRv, 216, 81
Alp, D., & Larsson, J. 2020, ApJ, 896, 39
An, T., Liu, Y., Feng, H., Tao, L., & Yuan, W. 2024, ATel, 16555, 1
Anderson, G. E., Horesh, A., Mooley, K. P., et al. 2017, MNRAS, 466, 3648
Andreoni, I., Coughlin, M. W., Kool, E. C., et al. 2021, ApJ, 918, 63
Andreoni, I., Coughlin, M. W., Perley, D. A., et al. 2022, Natur, 612, 430
Astropy Collaboration, Price-Whelan, A. M., Lim, P. L., et al. 2022, ApJ, 935, 167
Astropy Collaboration, Price-Whelan, A. M., Sipocz, B. M., et al. 2018, AJ, 156, 123
Astropy Collaboration, Robitaille, T. P., Tollerud, E. J., et al. 2013, A&A, 558, A33
Bauer, F. E., Treister, E., Schawinski, K., et al. 2017, MNRAS, 467, 4841
Belczynski, K., Askar, A., Arca-Sedda, M., et al. 2018, A&A, 615, A91
Bellm, E. C., Kulkarni, S. R., Graham, M. J., et al. 2019, PASP, 131, 018002
Berger, E., Kulkarni, S. R., Pooley, G., et al. 2003, Natur, 426, 154
Bloom, J. S., Giannios, D., Metzger, B. D., et al. 2011, Sci, 333, 203
Bright, J. S., Rhodes, L., Farah, W., et al. 2023, NatAs, 7, 986
Brown, G. C., Levan, A. J., Stanway, E. R., et al. 2015, MNRAS, 452, 4297
Buckley, D. A. H., Monageng, I., Aydi, E., Scaringi, S., & Charles, P. A. 2024, ATel, 16554, 1
Burrows, D. N., Kennea, J. A., Ghisellini, G., et al. 2011, Natur, 476, 421
Camilo, F., Scholz, P., Serylak, M., et al. 2018, ApJ, 856, 180
Carotenuto, F., Bright, J., Jonker, P. G., Fender, R., & Rhodes, L. 2024, GCN, 35961, 1
CASA Team, Bean, B., Bhatnagar, S., et al. 2022, PASP, 134, 114501
Cenko, S. B., Krimm, H. A., Horesh, A., et al. 2012, ApJ, 753, 77
Chambers, K. C., Magnier, E. A., Metcalfe, N., et al. 2016, arXiv:1612.05560
Chen, T. W., Yang, S., Lee, M. H., et al. 2024a, GCN, 35938, 1
Chen, T. W., Yang, S., Pan, Y. C., et al. 2021, TNSAN, 92, 1
Chen, Y., Jia, S. M., Cui, W. W., et al. 2024b, GCN, 35951, 1
Chevalier, R. A., & Fransson, C. 2008, ApJL, 683, L135
Chruslinska, M., Belczynski, K., Klencki, J., & Benacquista, M. 2018, MNRAS, 474, 2937
DeLaunay, J., Tohuvavohu, A., Svinkin, D., et al. 2024, GCN, 35971, 1
Eappachen, D., Jonker, P. G., Levan, A. J., et al. 2023, ApJ, 948, 91
Eappachen, D., Jonker, P. G., Quirola-Vásquez, J., et al. 2024, MNRAS, 527, 11823
Eldridge, J. J., Stanway, E. R., & Tang, P. N. 2019, MNRAS, 482, 870
Fletcher, C., Lesage, S., & Jenke, P. 2024, GCN, 35776, 1
Fong, W., Berger, E., Margutti, R., & Zauderer, B. A. 2015, ApJ, 815, 102
Gillanders, J. H., Troja, E., Fryer, C. L., et al. 2023, arXiv:2308.00633
Glennie, A., Jonker, P. G., Fender, R. P., Nagayama, T., & Pretorius, M. L. 2015, MNRAS, 450, 3765
Gompertz, B. P., Ravasio, M. E., Nicholl, M., et al. 2023, NatAs, 7, 67
Granot, J., & van der Horst, A. J. 2014, PASA, 31, e008
Groh, J. H., Meynet, G., & Ekström, S. 2013, A&A, 550, L7
Grupe, D., Nousek, J. A., Veres, P., Zhang, B.-B., & Gehrels, N. 2013, ApJS, 209, 20
Hanuschik, R. W. 2003, A&A, 407, 1157
Harris, C. R., Millman, K. J., van der Walt, S. J., et al. 2020, Natur, 585, 357
Heywood, I. 2020, oxkat: Semi-automated imaging of MeerKAT observations, Astrophysics Source Code Library, ascl:2009.003
Ho, A. Y. Q., Perley, D. A., Kulkarni, S. R., et al. 2020, ApJ, 895, 49
Ho, A. Y. Q., Phinney, E. S., Ravi, V., et al. 2019, ApJ, 871, 73
Hugo, B. V., Perkins, S., Merry, B., Mauch, T., & Smirnov, O. M. 2022, in ASP Conf. Ser. 532, ed. J. E. Ruiz, F. Pierfedereci, & P. Teuben (San Francisco, CA: ASP), 541
Hunter, J. D. 2007, CSE, 9, 90
Jonas, J. 2018, Proc. of MeerKAT Science: On the Pathway to the SKA — PoS (MeerKAT2016), 277 (Trieste: SISSA), 1
Jonker, P. G., Glennie, A., Heida, M., et al. 2013, ApJ, 779, 14
Kann, D. A., Klose, S., Zhang, B., et al. 2010, ApJ, 720, 1513
Labrie, K., Simpson, C., Cardenes, R., et al. 2023a, RNAAS, 7, 214

Labrie, K., Simpson, C., Turner, J., et al. 2023b, DRAGONS, v3.1.0, Zenodo, doi:10.5281/zenodo.7776065
Laskar, T., Alexander, K. D., Margutti, R., et al. 2023, ApJL, 946, L23
Leung, J. K., Ricci, R., Dobie, D., & Troja, E. 2024, GCN, 35968, 1
Levan, A. J., Gompertz, B. P., Salafia, O. S., et al. 2024a, Natur, 626, 737
Levan, A. J., Jonker, P. G., Malesani, D. B., et al. 2024b, GCN, 35963, 1
Levan, A. J., Jonker, P. G., Malesani, D. B., et al. 2024c, GCN, 35982, 1
Levan, A. J., Tanvir, N. R., Cenko, S. B., et al. 2011, Sci, 333, 199
Levan, A. J., Tanvir, N. R., Starling, R. L. C., et al. 2014, ApJ, 781, 13
Ling, Z. X., Liu, M. J., Liu, Y., et al. 2024, ATel, 16546, 1
Liu, M. J., Li, D. Y., Liu, Y., et al. 2024a, ATel, 16514, 1
Liu, Y., Liu, M. J., Cheng, H. Q., et al. 2024b, ATel, 16509, 1
MacLeod, M., Trenti, M., & Ramirez-Ruiz, E. 2016, ApJ, 819, 70
Madau, P., & Dickinson, M. 2014, ARA&A, 52, 415
Magnier, E. A., Chambers, K. C., Flewelling, H. A., et al. 2020a, ApJS, 251, 3
Magnier, E. A., Schlafly, E. F., Finkbeiner, D. P., et al. 2020b, ApJS, 251, 6
Magnier, E. A., Sweeney, W. E., Chambers, K. C., et al. 2020c, ApJS, 251, 5
Mapelli, M., & Giacobbo, N. 2018, MNRAS, 479, 4391
Mazzali, P. A., Valenti, S., Della Valle, M., et al. 2008, Sci, 321, 1185
McKinney, W. 2010, in Proc. of the 9th Python in Science Conf., ed. S. van der Walt & J. Millman, 56
Modjaz, M., Li, W., Butler, N., et al. 2009, ApJ, 702, 226
Moldon, J. 2021, eMCP: e-MERLIN CASA pipeline, Astrophysics Source Code Library, ascl:2109.006
Monageng, I. M., Charles, P. A., Buckley, D. A. H., et al. 2024, ATel, 16529, 1
Murakami, T., Inoue, H., Nishimura, J., van Paradijs, J., & Fenimore, E. E. 1991, Natur, 350, 592
Nicholl, M., Srivastav, S., Fulton, M. D., et al. 2023, ApJL, 954, L28
Offringa, A. R., McKinley, B., Hurley-Walker, N., et al. 2014, MNRAS, 444, 606
pandas development team, T. 2020, pandas-dev/pandas: Pandas, latest, Zenodo, doi:10.5281/zenodo.3509134
Pasham, D. R., Lucchini, M., Laskar, T., et al. 2023, NatAs, 7, 88
Piro, L., De Pasquale, M., Soffitta, P., et al. 2005, ApJ, 623, 314
Planck Collaboration, Ade, P. A. R., Aghanim, N., et al. 2016, A&A, 594, A13
Prentice, S. J., Maguire, K., Smartt, S. J., et al. 2018, ApJL, 865, L3
Quirola-Vásquez, J., Bauer, F. E., Jonker, P. G., et al. 2022, A&A, 663, A168
Quirola-Vásquez, J., Bauer, F. E., Jonker, P. G., et al. 2023, A&A, 675, A44
Quirola-Vásquez, J., Jonker, P. G., Levan, A. J., et al. 2024, GCN, 35960, 1
Racusin, J. L., Karpov, S. V., Sokolowski, M., et al. 2008, Natur, 455, 183
Rastinejad, J. C., Gompertz, B. P., Levan, A. J., et al. 2022, Natur, 612, 223
Rhodes, L., Bright, J. S., Fender, R., et al. 2023, MNRAS, 521, 389
Ricci, R., Dobie, D., Leung, J. K., & Troja, E. 2024, GCN, 35990, 1
Rodriguez, A., & Kulkarni, S. R. 2024, ATel, 16549, 1
Saccardi, A., Levan, A. J., Zhu, Z., et al. 2024, GCN, 35936, 1
Santoliquido, F., Mapelli, M., Giacobbo, N., Bouffanais, Y., & Artale, M. C. 2021, MNRAS, 502, 4877
Sari, R., Piran, T., & Halpern, J. P. 1999, ApJL, 519, L17
Sarin, N., Ashton, G., Lasky, P. D., et al. 2021, arXiv:2105.10108
Schlafly, E. F., & Finkbeiner, D. P. 2011, ApJ, 737, 103
Smith, K. W., Smartt, S. J., Young, D. R., et al. 2020, PASP, 132, 085002
Soderberg, A. M., Berger, E., Page, K. L., et al. 2008, Natur, 453, 469
Srivastav, S., Smartt, S. J., Fulton, M. D., & Smith, K. W. 2024a, GCN, 35933, 1
Srivastav, S., Smartt, S. J., Fulton, M. D., et al. 2024b, GCN, 35932, 1
Stalder, B., Tonry, J., Smartt, S. J., et al. 2017, ApJ, 850, 149
Steele, I. A., Smith, R. J., Rees, P. C., et al. 2004, Proc. SPIE, 5489, 679
Sun, H., Wang, C. W., Yang, J., et al. 2023, arXiv:2307.05689
Svinkin, D., Frederiks, D., Lysenko, A., et al. 2024a, GCN, 35972, 1
Svinkin, D., Frederiks, D., Ridnaia, A., et al. 2024b, GCN, 35966, 1
Tauris, T. M., Kramer, M., Freire, P. C. C., et al. 2017, ApJ, 846, 170
Tonry, J., Denneau, L., Weiland, H., et al. 2024, TNSTR, 2024-715, 1
Tonry, J. L., Denneau, L., Flewelling, H., et al. 2018a, ApJ, 867, 105
Tonry, J. L., Denneau, L., Heinze, A. N., et al. 2018b, PASP, 130, 064505
Tonry, J. L., Stubbs, C. W., Kilic, M., et al. 2012a, ApJ, 745, 42
Tonry, J. L., Stubbs, C. W., Lykke, K. R., et al. 2012b, ApJ, 750, 99
Troja, E., Fryer, C. L., O'Connor, B., et al. 2022, Natur, 612, 228
van der Horst, A. J., Kamble, A., Resmi, L., et al. 2008, A&A, 480, 35
Vestrand, W. T., Wozniak, P. R., Wren, J. A., et al. 2005, Natur, 435, 178
Vigna-Gómez, A., Neijssel, C. J., Stevenson, S., et al. 2018, MNRAS, 481, 4009
Wang, X.-G., Zhang, B., Liang, E.-W., et al. 2018, ApJ, 859, 160
Waters, C. Z., Magnier, E. A., Price, P. A., et al. 2020, ApJS, 251, 4
Xue, Y. Q., Zheng, X. C., Li, Y., et al. 2019, Natur, 568, 198
Yang, J., Ai, S., Zhang, B.-B., et al. 2022, Natur, 612, 232
Yang, S., Sollerman, J., Chen, T. W., et al. 2021, A&A, 646, A22
Yang, Y.-H., Troja, E., O'Connor, B., et al. 2024, Natur, 626, 742
Yao, Y., Lu, W., Harrison, F., et al. 2024, ApJ, 965, 39
Yuan, W., Zhang, C., Chen, Y., & Ling, Z. 2022, The Einstein Probe Mission (Singapore: Springer Nature), 1
Zauderer, B. A., Berger, E., Soderberg, A. M., et al. 2011, Natur, 476, 425
Zhang, B., Sun, H., Yin, Y.-H. I., et al. 2024a, GCN, 35773, 1
Zhang, C., Ling, Z. X., Liu, Y., et al. 2024b, ATel, 16463, 1
Zhang, W. J., Mao, X., Zhang, W. D., et al. 2024c, GCN, 35931, 1